Chapter 5

Mechanically Flexible Au-Ag Bimetallic Transparent Conducting Thin Film and its Application as Self-Bias Plasmonic NIR Photodetector

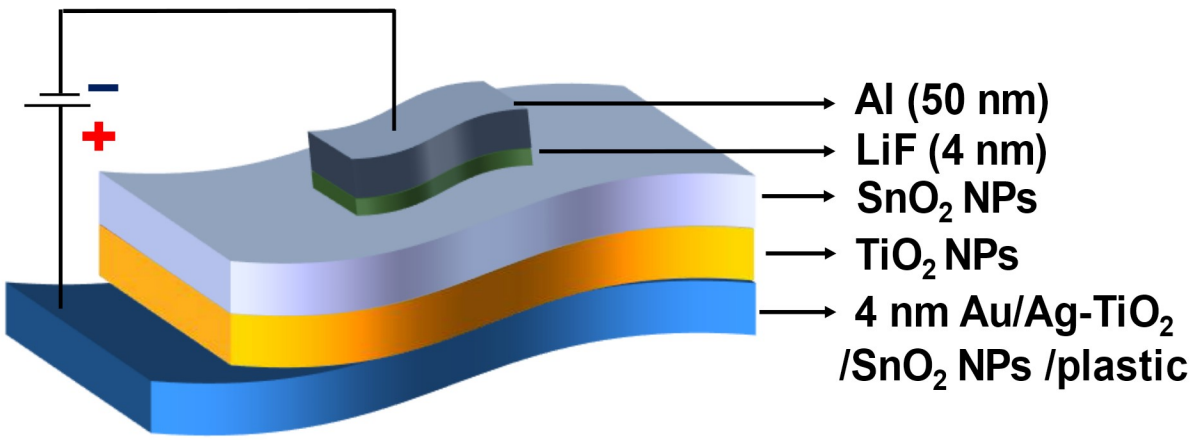

Chapter 5

This chapter mainly focuses on development of a bimetallic Au-Ag TC film fabrication method and its use as a self-bias plasmonic NIR photodetector. This is a follow-up work of the earlier chapter for developing TC and its application. Here, a 4 nm PVD deposited Au is grown on a pre-deposited Ag-TiO_2/SnO_2 (or ZnO NPs) thin film that enhances the transparency, conductivity and environmental stability of the TC. This Ag-TiO_2 thin film is a Ag nanoparticle embedded TiO_2 thin film that has been grown over SnO_2 (or ZnO NPs) which leads to a percolated nano-porous-like structure. Prior to this, surface morphology of the film shows a clear transition from spherical NPs to percolated nano-porous Au-Ag bimetallic nanostructure with random hole formation that result in an abrupt jump of electrical conductivity when deposition reaches to 4 nm mass thickness of Au. This percolated nano-porous structure thin film (4 nm Au/Ag-TiO_2/SnO_2 (or ZnO NPs) /plastic) has a low resistivity of ~ 10-15 ohm/□ and an average visual transmittance around 75-80 % in the visible region. This film has been used to develop a metal-semiconductor-metal (M-S-M) plasmonic hot electron photodetectors where Au-Ag thin film works as a photo-excited hot electron generation as well as transparent bottom electrode. The EQE data reveal that photocurrent of this device is mostly generated in the plasmonic absorption region with a peak detectivity of 1.6×10^{13} Jones at 750 nm under -2V external bias. Besides, the device shows fast response with a response time of ~33 ms.

5.1 Introduction

Plasmonic Transparent Conductors (TCs) are an essential component in many opto-electronic devices, such as touch screens, wearable sensors, memory device, Organic Light-Emitting Diodes (OLED), solar cells, and smart windows.[244-250] Over the past few decades, Indium Tin Oxide (ITO) and Fluorine Tin Oxide (FTO) based materials have played a major role in the current market share due to its high optical transparency (T~90%) and low sheet resistance (R_s <100 Ω/□).[116, 117] On the other hand, indium is not an abundant materials.[119] It has a few limited applications because of its low resistance to mechanical

stress (lack of flexibility) and a difficult manufacturing process.[118] In the last decade, tremendous efforts have been admired for the development of next generation transparent conductive films. Among various options, carbon nanotube or graphene has higher mechanical flexibility as well as optical transparency.[175, 176, 251] Although, the electrical conductivity of these ITO or carbon-based TCs is quite lower with respect to metals like Ag, Cu, and Au. So, metal nanoparticles or metal nanowire networks are emerging as a promising alternative to ITO, especially in flexible and stretchable electronics.[252, 253] This is mainly because of their superior mechanical flexibility, high optical quality, low sheet resistance, and low production costs. Among different metals, Ag has the highest intrinsic conductivity and least refractive index (n) in the visible region compared to Cu or Au. Therefore, the development of TC material is often accomplished in the majority of those investigations using either Ag nanowire or oxide/Ag/oxide multi-stack thin film.[181, 254, 255] Even in so many reports, Cu nanowires are also well studied for developing TC material.[256] But both Ag and Cu individually show poor chemical stability against oxidation.[257, 258] On the other hand, Au shows the highest chemical stability, but it shows the least intrinsic conductivity compared to Ag or Cu. Considerable research has been devoted to solving this issue, mostly by exploiting a core−shell structure that encapsulates metals with an inert shell which is a cost-effective process.[259, 260]

The overgrowth of a metal onto the surface of another metal represents a synthetic challenge. **Yuan et al**. revealed that the galvanic reaction between Ag and $HAuCl_4$ could be blocked in the presence of strong reducing agents.[261] There are very few papers that describe the development of TC material using bimetallic Au-Ag, Ag-Cu, or Au-Cu core structures. Despite the encouraging progress in the literature, it's important to fabricate TC material that shows excellent optical transparency, electrical conductivity, mechanical flexibility as well as chemical stability against oxidation. However, these thin metal films have very strong plasmonic absorption which is a key barrier to achieving high optical transparency of those films.[123, 184]

Although plasmonic absorption is a key bottleneck in developing metal-based highly transparent conductors, it's useful for developing various opto-electronic devices including solar cells, plasmonic photodetectors, gas sensors, and LEDs.[186, 189, 192] So many

reports claim that the plasmonic effect of those transparent electrodes can generate hot-electron induced photocurrent which can be beneficial for photocurrent generation of solar cells, photodetector, and photo-electrochemical H_2 generation.[190, 191] When EM waves interact with MNPs, part of that EM waves is scattered and the rest of the part is absorbed by MNPs due to the SPR. This SPR absorption of MNPs increases whereas scattering reduces with reducing particle size. Besides, the shape of metal NP, the relation of dielectric constant of MNPs, and surrounding are also important parameters for SPR related absorption of MNPs.[81] Due to the SPR, MNPs either generate electron-hole pairs or go through radiative decay to the far field. Again, this generated electron-hole pair can produce hot-electron through non-thermal electron distribution via electron-electron scattering. To utilize this hot-electron for optoelectronics device application, a semiconductor-metal Schottky junction is required through which it can be injected into the semiconductor within a very short period (<100 fs), before non-radiative energy relaxation of hot-electron through electron-phonon scattering. Besides, for efficient electron injection of this hot-electron in the Schottky junction, a low barrier height (Φ_b) Schottky junction is required.[154] In plasmonic devices, this metal-semiconductor Schottky junction has been developed by varsities ways like; by depositing a metal thin film on a nanostructured semiconductor surface followed by inert atmosphere annealing to form MNPs, MNPs-metal oxide thin film, semiconductor-metal thin film hetero-junction etc.[195, 199] Therefore, Au-Ag bimetallic nanostructures can provide a combined effect of both metallic properties. Interestingly, Ag nano-structures allow the growth of Au NPs on their surface due to the same lattice match between their crystal structures, leading to the synthesis of bimetallic nanostructures. The growth of Au NPs onto another metal surface like Ag NPs leads to the creation of different dipolar and multipolar LSPR. Directed overgrowth of Au on Ag can tune nanostructured SPR from visible to NIR region. This overgrowth of Au is highly dependent on the core Ag geometry. By varying the amount of metal NPs used during the growth process, SPR can be tuned towards NIR which leads NIR sensitive plasmonic photodetector, SERS based applications.[262, 263] In addition, several reports claim that the opto-electronic devices performance can be improved by using a plasmonic electrode. In a plasmonic photodetector, the contribution of hot electrons is commonly realized from the external quantum efficiency (EQE) measurement that indicates a strong photocurrent generation in the plasmonic absorption region of MNPs.

However, there are very limited reports that demonstrate identical plasmonic absorption and EQE spectra of the device. Moreover, those devices show quite poor response for different plasmonic photodetector applications.

This chapter reports the synthesis of Au-Ag bimetallic transparent conducting film on plastic substrate at a low processing temperature (100˚C). The as-synthesized Au-Ag bimetallic thin film is highly conductive with sheet resistance as low as 5-10 Ω/□ with more than 80% transparency. At the initial stage of the growth, it has been observed that the nucleation density of Au on this substrate is much higher than bare plastic substrate which are originated by pre-deposited Ag islands of the Ag-TiO_2 film. However, after a critical size growth of those grains, granular film undergoes a solid-state dewetting process which makes it possible to deposit percolated finger-like Au-Ag nanostructured thin film. As a consequence, the resistivity of the film dropped suddenly. Besides, due to the lower mass thickness of Au film, transparency has been maintained over 80% in the visible region. However, it drops to ~50-60% in the higher wavelength region of light due to the plasmonic absorption of the film. To analyze the surface phenomena of this percolated finger-like Au-Ag nanostructured we developed a percolation model which tells about the nature of percolation threshold during growth. Besides, this transparent-conducting Au-Ag bimetallic film has been used as a plasmonic electrode for developing high performance hot-electron photodetectors. The device has been fabricated on the same plastic substrate as well as a highly doped silicon (n^+- Si) substrate that shows extremely high detectivity with fast response speed. The UV-Vis absorption spectra of Au-Ag bimetallic TC film show a strong SPR absorption from visible to NIR region which has an excellent spectral matching with the EQE spectra of the photodetector, implying the major contribution of hot-electron in the photocurrent generation of the device.

.

5.2 Experimental Section

5.2.1 Preparation of Precursor Materials

The preparation process for SnO_2 NPs, ZnO NPs, TiO_2 NPs and ion-conducting dielectric LTO via low temperature solution process technique has been explained in **Chapter 2 Section 2.1.3, 2.1.4, 2.1.6 and 2.1.1.**

5.2.2 Fabrication of Au-Ag TC Film and Plasmonic NIR Photodetector

Bimetallic Au-Ag based TC film has been fabricated on a flexible PET substrate and the fabrication steps has been explained **Chapter 2 Section 2.3.3**, and schematically present in **Figure 2.9**. For fabrication of a photodetector, these optimized mechanically flexible bimetallic Au-Ag TC thin film have been used as transparent bottom electrode to develop NIR active plasmonic photodetector in a photodiode geometry which is schematically present in **Figure 2.10**.

5.3 Results and discussion

5.3.1 Electrical and Optical Characterization of Flexible Au-Ag Bimetallic Transparent Conductor

To measure the electrical conductivity of prepared Au-Ag TC films, parallel Ag electrodes (thickness ~ 50 nm) of separation 0.45 mm have been deposited over the conductive film. **Figure 5.1a)** depicts the semi-log plot of current density vs voltage (J-V) graphs of those 4 nm Au/Ag-TiO_2 thin films with SnO_2 or ZnO NPs. This data implies that conductivity of 4 nm Au/Ag-TiO_2 film with SnO_2 NPs is higher w.r.t ZnO NPs. Besides, it can be noted that a significant quantity of current (~ mA) is produced by applying a relatively modest voltage of 0.05 V. Besides, to test the flexibility of the prepared film, we examined the conductivity of our best performed device (4 nm Au/Ag-TiO_2/SnO_2 NPs) with different bending cycles in **Figure 5.1b)** upto 100 (bending radius ~ 4 mm). This study indicates that conductivity of the film remains almost unaltered even after 100 cycles of bending, which implies this conductor is suitable for fabrication of flexible photo-voltaic devices.

The optical transparency of the 4 nm Au/Ag-TiO_2 thin films with SnO_2 or ZnO NPs has been investigated and is shown in **Figure 5.1c)**. This data implies that the 4 nm Au/Ag-TiO_2/SnO_2

NPs conductor has an excellent optical transparency of ~ 80-82 %, where ZnO NPs based device shows an optical transparency around 76-78 % in the wavelength region of 500-600 nm. As film is showing better transparency and conductivity with SnO_2 NPs compare to ZnO NPs, for other characteristic we mainly go through SnO_2 NPs compatible TC film. For longer wavelengths, films transparency is reduced to ~ 65-70 %. The reduction of transparency arises mainly due to the plasmonic absorption of the film. The phenomena of conductivity and transparency are interconnected for any TC devices. Besides, resistance vs temperature of (4 nm Au/Ag-TiO_2/SnO_2 NPs) samples has been measured by four probe methods. The sample shows moderate drop in resistance upto 200 K which indicates fully metallic behavior of the film **Figure 5.1d)**.

The precise form of this dependency is defined by the impact of varying deposition conditions on the electro-optical characteristics of these layers. However, for any conducting film sheet resistance (R_{sh}) is an important measurement. Our calculated R_{sh} for both films are listed below in **Table 5.1.** The **Figure 5.1e)** shows the real picture of comparative transparency of the 4 nm Au/Ag-TiO_2/SnO_2 NPs w.r.t references. Our reference Device (4 nm Au/plastic) and only plastic film transparency spectra are given in (**Figure 5.2**).

Table 5.1 Electrical Sheet Resistance and Visible Transmittance Value of Mechanically Flexible Au-Ag TC Film

Au-Ag bi-metallic film	Sheet Resistance (Ω/□)	Visible Transmittance (%) λ= 550 nm
4 nm Au/Ag-TiO_2/SnO_2 NPs	5.37	81.48 %
4 nm Au/ Ag-TiO_2/ZnO NPs	14.63	77.69 %

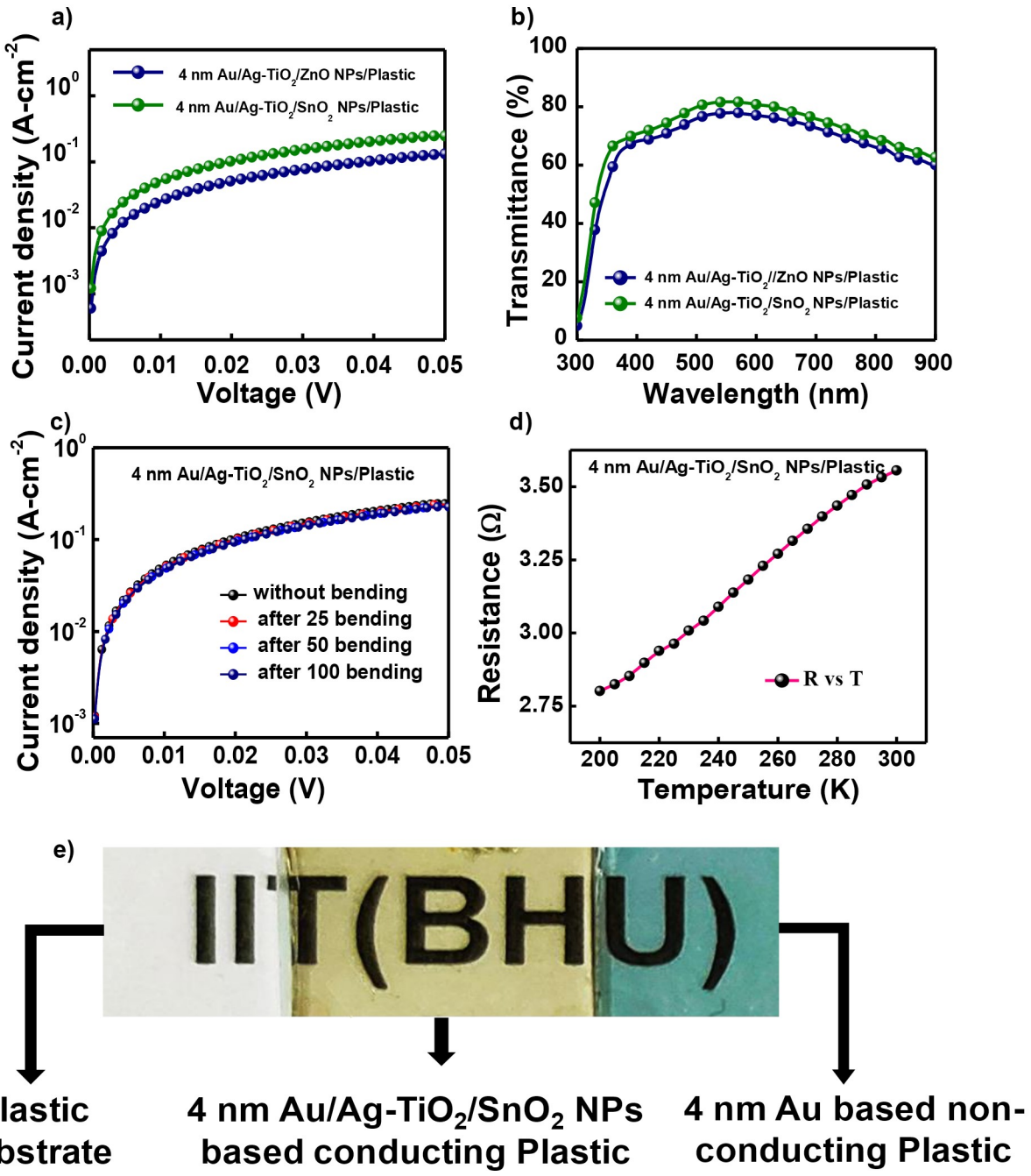

Figure 5.1a) Semi-log graph of electrical current density vs voltage of 4 nm Au/Ag-TiO_2 based transparent conducting film with SnO_2 or ZnO NPs **b)** mechanical flexibility upto 100 bending cycles (bending radius 4 mm) **c)** optical transparency of TC film with two different film, **d)** variation of R vs. T using four-probe low temperature set-up and **e)** real picture of TC film with reference.

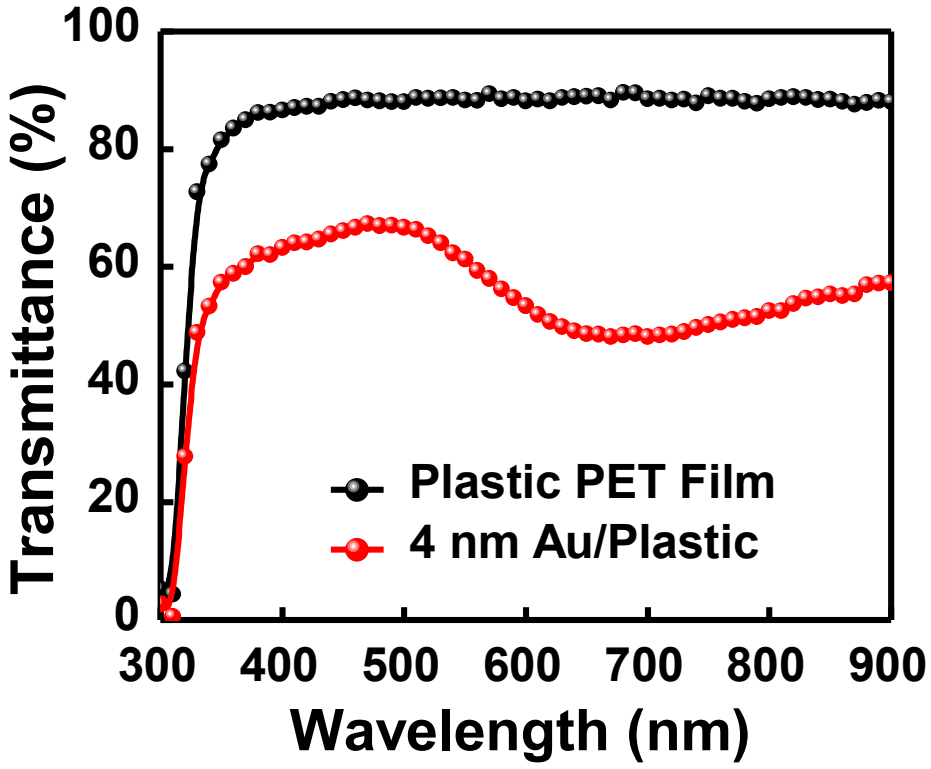

Figure 5.2 Transparency Spectra of 4 nm Au/plastic and plastic PET substrate.

5.3.2 XRD, Raman, UV-NIR absorption & PL Spectra

Figure 5.3a) depicts step-by-steps XRD pattern of the thin films that are deposited in the similar way that followed to fabricate Au-Ag bimetallic based nanostructured thin film. A bare plastic substrate is used as a reference, and the XRD data of the bare plastic is subtracted from sample data to get the actual signal of the sample. The XRD pattern of SnO_2 NPs thin films annealed at 100°C exhibits peak position located at 2θ of 26.17°, 33.58°, 51.47° and 54.45° which corresponds to (110), (101), (211), and (310) planes respectively, indicating the formation of crystalline phase of SnO_2 NPs thin film over the substrate (JCPDS file no. 411445). In next step, thin-film XRD pattern of LTO/SnO_2 NPs shows two additional intense peaks of LTO at 2θ ~ 35.77° and 43.52°, which has come from the reflection planes of (311) and (400) respectively (JCPDS file no. 490207). After ion-exchange process of this, film shows extra three intense peaks at 2θ ~ 25.1°, 37.84° and 44.02° which corresponds to anatase TiO_2 (101), Ag (111) and Ag (200) respectively (JCPDS file no 897322 & 731764). These intense broad peaks of Ag NPs are confirming the formation of Ag

NPs inside TiO_2 matrix after ion-exchange process. At final stage, TC thin film (4 nm Au/Ag-TiO_2 /SnO_2 NPs) thin film shows similar peak positions with much higher intensity at 2θ ~ 37.84˚, and 44.02˚. These peak positions of Au or Ag NPs are common because of their very similar lattice parameters. From this XRD spectra its very clear that the width of the peaks is quite wide, indicates the small size of the metal/metal oxide nanoparticle.

Figure 5.3b) shows the Raman spectra of 4 nm Au/Ag-TiO_2/SnO_2 NPs thin film. From this study an intense peak has been observed at 630 cm^{-1} which originated from the SnO_2 NPs. The peak position at 1086, 1193 and 1616 cm^{-1} which corresponds to Au or Ag NPs and the rest peaks at 705, 865, 995, 1293 and 1729 cm^{-1} corresponds to plastic substrate. This Raman data confirms the formation of Au-Ag bimetallic conducting film on plastic. For optical studies, the thin film of 4 nm Au/Ag-TiO_2/SnO_2 NPs is fabricated on a quartz substrate. The normalized UV-Vis absorbance spectra of Au/Ag-TiO_2/SnO_2 NPs thin films spanning the optical spectral region of 300–1800 nm are shown in **Figure 5.3c)**. The absorption spectrum of as-prepared 4 nm Au/Ag-TiO_2/SnO_2 NPs thin films demonstrate a spectrally broadened spectrum from UV-Vis to NIR region with a plasmonic peak around 750 nm wavelength whereas the reference Au NPs film shows plasmonic peak ~ 520-560 nm in visible range of spectra., implying a red shift of >200 nm of the plasmonic peak due to the Au-Ag bimetallic nanostructure formation (**Figure 5.3c)).** The plasmonic absorption in the NIR region appeared due to the longitudinal plasmon mode of the porous Au-Ag bimetallic nano-film formed during the lateral growth of Au NPs over Ag-TiO_2/SnO_2 NPs surface. The PL spectra of the 4 nm Au/Ag-TiO_2/SnO_2 NPs thin film is shown in **Figure 5.3d)** which is acquired in the range of 320-550 nm with an excitation wavelength of 300 nm, indicating the emission peaks around 370 nm (3.35 eV), which is directly providing the energy band gap of the thin film. The PL peak position at 370 nm suggests specific optical properties that could be attributed to the formation of an Au-Ag bimetallic nanostructure on TiO_2/SnO_2 matrix. Pure Au or Ag NPs typically have PL characteristics with a peak position of much larger wavelength, indicating a possible radiative recombination through intermetallic energy states.

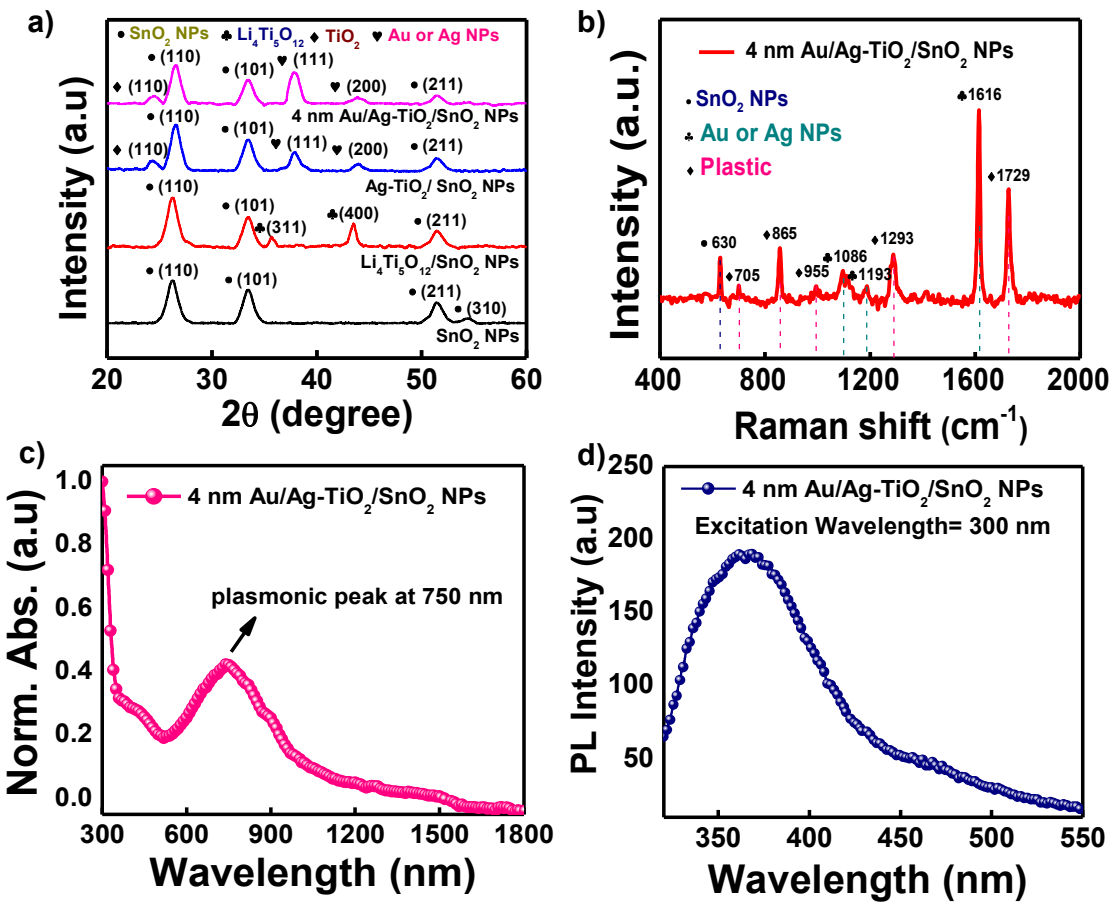

Figure 5.3 Structural analysis of 4 nm Au/Ag-TiO_2/SnO_2 NPs thin film **a)** XRD Spectra **b)** Raman Spectra **c)** UV-Vis-NIR absorption Spectra, and **d)** PL Spectra.

5.3.3 Surface Morphology (HR-SEM & AFM) Study

The surface morphology of Au/Ag-TiO_2/SnO_2 NPs thin film on plastic substrates are studied by HR-SEM. **Figure 5.4a,b&c)** demonstrated the morphological change of the films with the increasing mass thickness of thermally deposited Au film over Ag-TiO_2/ SnO_2 NPs thin film. From this surface morphology study, it's very clear that the individual islands (**Figure 5.4a)** to a percolated network (**Figure 5.4b)** transition is occurring during the process with a critical mass thickness of 4 nm..[200, 201] Although this phase transition of the surface morphology is not observed in the reference 4 nm Au film over bare plastic substrate **(Figure 5.7a)**. From this comparative study, it can be speculated that the morphological phase transition of 4 nm Au/Ag-TiO_2/SnO_2 NPs film occurs due to the coalescence of individual grains with their neighbor which becomes possible due to the pre-existing Ag NPs of Ag-

TiO_2 film which is grown during the ion-exchange process. Due to this low mass thickness of Au film, optical transparency is very high by maintaining its metallic conductivity. Moreover, these nano-porous structures can create intrinsic EM hot spots which leads to produce a highly sensitive plasmonic opto-electronic device. Further deposition of Au film (~ 6 nm) covers the voids (**Figure 5.4c)**), as a result film will become more electrically conducting but transparency decreases drastically. An energy- dispersive X-ray spectrometer (EDX) & color-mapping attached to the HR-SEM instrument is used to figure out the contents and amount of metallic elements present in 4 nm Au/Ag-TiO_2/ SnO_2 NPs is shown in **Figure 5.5**, which confirms the presence of Au, Ag, Ti, Sn and O uniformly throughout the film.

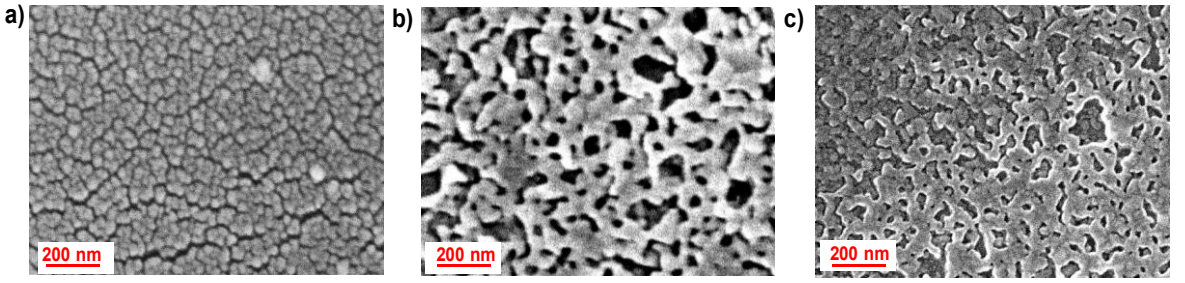

Figure 5.4 FE-SEM photographs of Au/Ag-TiO_2/SnO_2 NPs thin film at room temperature on plastic. Each photograph's average film thickness is listed below. **a)** shows the early stage of growth and coalescence of islands **b)** percolating nano-porous structures **c)** complete percolating structures

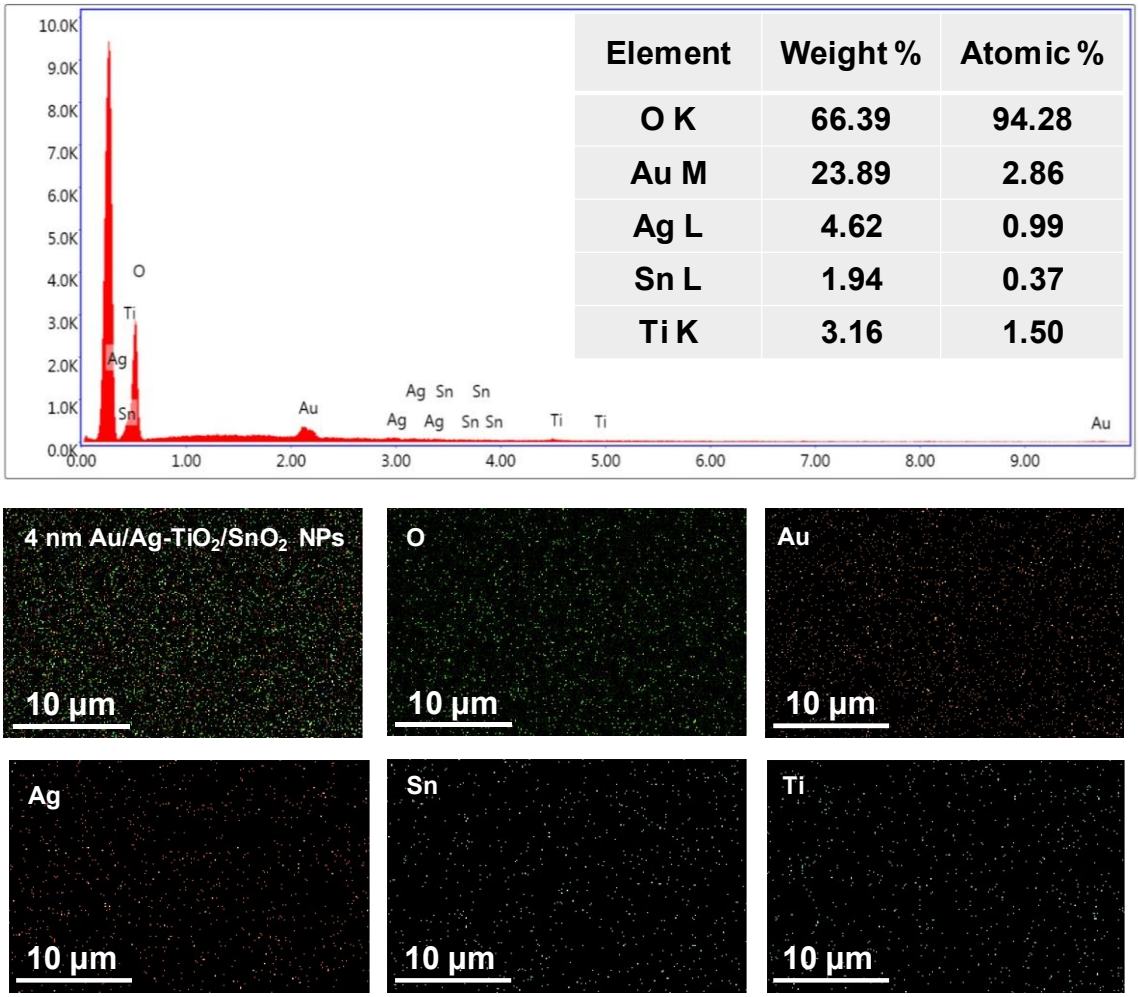

Figure 5.5 Energy dispersive spectra of 4 nm Au/Ag-TiO_2/SnO_2 NPs/plastic thin film, with the elemental composition determined by EDX displayed in the inset. Color mapping of (i) 4 nm Ag/Ag-TiO_2/SnO_2 NPs thin film (ii) O, (iii) Au, (iv) Ag, (v) Sn, (vi) Ti.

Furthermore, AFM has been used for more detailed surface study of Au/Ag-TiO_2/ SnO_2 NPs thin films to recognize the surface roughness (R_{rms}) shown in **Figure 5.6a,b&c)**. These studies show that the surface roughness for 2 nm Au/Ag-TiO_2/SnO_2 NPs is quite low (R_{rms} ~ 1.55 nm) as film is fully covered by individual tiny NPs, but as soon as mass thickness reached 4 nm, film goes through a phase transition from individual metallic islands to a percolated nano-porous type structure which create denser EM hotspot and multipolar resonance effect. As a result, films surface roughness increases quite significantly to 3.91 nm. On the other hand, in case of 6 nm Au/Ag-TiO_2/SnO_2 NPs (R_{rms} ~1.62 nm), further

growth covers the porosity of the film, reduces its surface roughness to 1.62 nm. Besides, **Figure 5.6d,e&f)** shows the 3-D AFM images of the film for more celerity. The 2D-AFM image of reference 4 nm Au (R_{rms} ~ 5.74 nm) on the bare plastic substrate is shown in **Figure 5.7b)**, indicates its larger roughness.

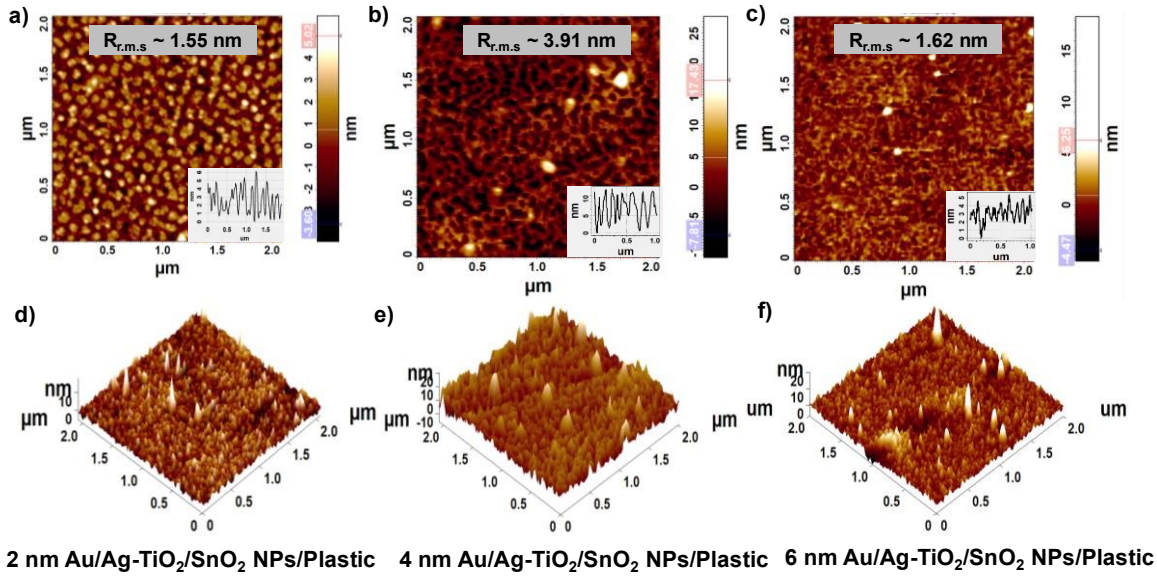

Figure 5.6a,b&c) 2-D AFM & **d,e&f)** 3D-AFM image of (2 or 4 or 6 nm Au)/Ag-TiO_2/SnO_2 NPs. Each rms roughness is listed in the graphics.

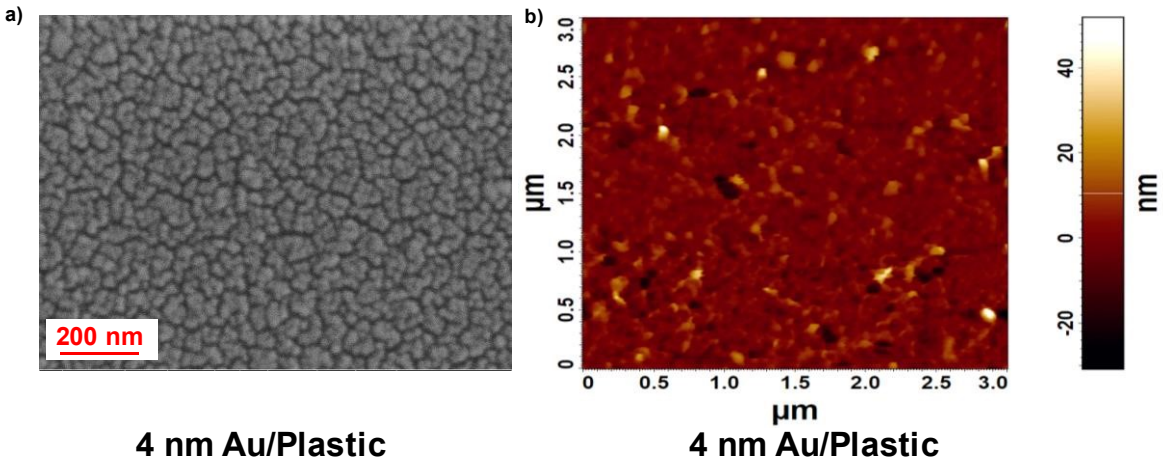

Figure 5.7 a&b) HR-SEM and 2D-AFM image of 4 nm Au reference thin film on plastic.

5.3.4 HR-TEM Study

Figure 5.8a)shows a TEM study of the 4 nm Au/Ag-TiO_2/SnO_2 NPs nanocomposites for further structural analysis. To prepare the TEM sample, the film is scratched off with a clean glass slide and placed on clean paper. Following that, it is dissolved in isopropyl alcohol and dispersed for a few minutes using a probing sonicator. A drop of this dispersed material is then collected and placed on a TEM grid. **Figure 5.8a)** shows that the Au or Ag NPs have grown quite uniformly within the TiO_2/SnO_2 NPs matrix. These data also show that the NPs are predominantly between 5 and 15 nm in size, with an average particle size of 8.84 nm. The particle size distribution of Au or Ag NPs inside the TiO_2/SnO_2 NPs matrix is shown in **Figure 5.8b)**. Higher-magnification TEM analysis **Figure 5.8c)** of 4 nm Au/Ag-TiO_2/SnO_2 NPs sample indicates individual lattice fringe formation of Au or Ag NPs and inside the TiO_2/SnO_2 NPs, implying their own coexistence. The average d spacing's of Au or Ag NPs and SnO_2 NPs are 0.213, 0.242, and 0.348 nm, respectively, which correspond to the Au or Ag (200), Au or Ag (111), and SnO_2 NPs (101) planes. All of these spacing's are also defined by the selected-area electron diffraction (SAED) pattern, as shown in **Figure 5.8d)**. As shown earlier, the XRD pattern of the 4 nm Au/Ag-TiO_2/SnO_2 NPs sample (**Figure 5.3a)**) also reveals the same set of planes.

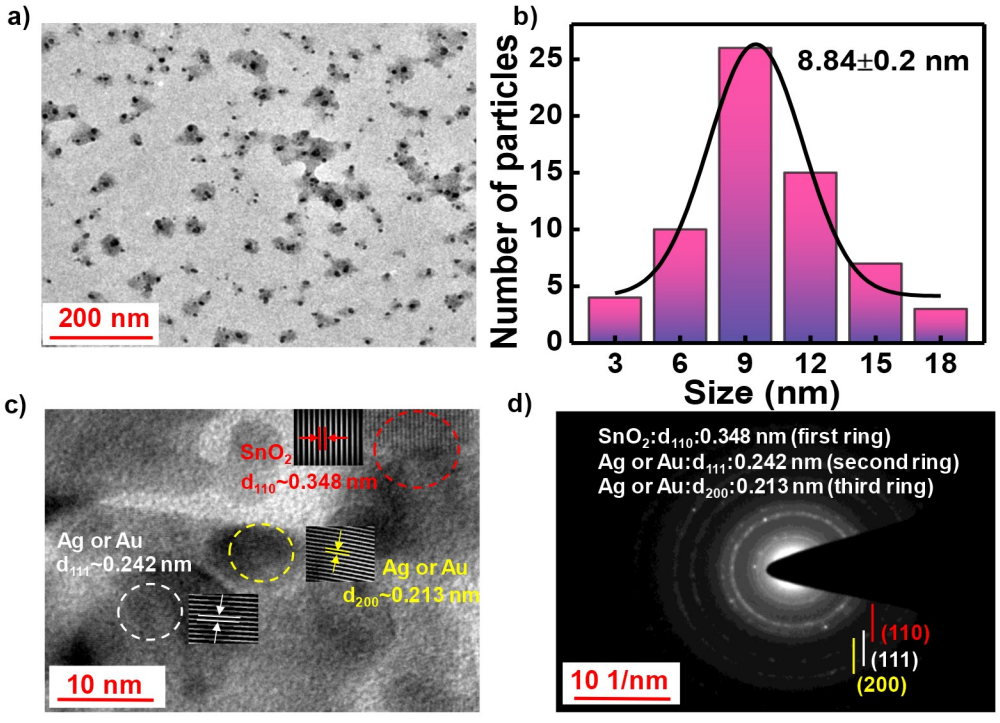

Figure 5.8 a) TEM image of 4 nm Au/Ag-TiO_2/SnO_2 NPs **b)** distribution of the particle sizes of Au or Ag NPs from the TEM image **c&d)** high-resolution TEM image and SAED pattern of 4 nm Au/Ag-TiO_2/SnO_2 NPs film.

5.3.5 Optoelectronics characterization of the photodetectors

As mentioned earlier, plasmonic photodetectors have been fabricated in a cross-bar geometry with the help of multilayer stack-structure of (LiF/Al)/SnO_2 NPs/4 nm Au/Ag-TiO_2/ plastic where 4 nm Au/Ag-TiO_2 works as bottom transparent electrode and LiF/Al works as a top electrode with an active area of 1×1 mm^2. Photocurrent of this device is generated from the hot electron generated due to the LSPRs effect of nano-porous Au-Ag thin film. The surface conduction electrons of Au or Ag NPs that collectively oscillate in response to incident light, leading to enhanced EM fields near the NPs. This enhanced EM field leads to the absorption of incident photons resulting in the generation of hot electrons. During electrical characterization of the device, white light of different intensity has been illuminated from the back side of the device that partly transmits and partly absorbed by 4 nm Au/Ag-TiO_2/SnO_2 NPs electrode due to the semi-transparent nature and plasmonic absorption of the electrode respectively in longer wavelength region. **Figure 5.9a)** shows the semi-log plot of electrical current-voltage parameters of this plasmonic photodetector device under dark and light. From this figure, it is clear that the device is rectifier in nature and reverse photocurrent increases with light intensity. When the light intensity is varied from 0 to 400 W/m^2, with moderate reversed bias current at 1V, increases from ~1.8×10^{-9}A to ~9.98×10^{-8}A, which 55 times w.r.t the dark current. Besides, I−V characterization data are plotted in a linear scale **Figure 5.9b)**, which ensures the device is a diode in nature. Furthermore, it has been observed that the reverse bias photocurrent variation is nearly linear (LDR curve) with the incident light intensity (**Figure 5.9c)**). Barrier height and ideality factor of the proposed device under light condition is calculated using **Equation 2.7** and **2.8** respectively. The calculated value of ideality factor and barrier height under different light intensities are plotted in **Figure 5.10a&b)**. Under dark, the ratio of forward bias to reverse bias current (rectifying ratio) is quite high at 1 V is ~1800. With different light intensities rectifying ratio is plotted in **Figure 5.10c)**. **Figure 5.9d)** shows schematic representations of the relative energy band structure, band bending, and charge separation of these devices under

illumination. As soon, light is illuminated, the bottom 4 nm Au/Ag-TiO_2/SnO_2 NPs electrode generates a hot-electron due to the plasmonic absorption and subsequently transfers to the CB of TiO_2 and SnO_2 NPs and finally reaches to the CB of LiF/Al. Hole, on the other hand, is collected by the Au-Ag bimetallic electrode itself. The concept of using LiF/Al as a top electrode to increase the work function between top and bottom electrode. Al electrode has work function of 4.1 eV but if we use an interface layer of LiF it decreases to 3.75 eV.[264] On the other hand, Au-Ag bimetallic electrode has a work function around 4.9 eV. This generates electron-hole pairs that are separated due to the built-in electric field within the photodiode structure and the different work functions of the electrode materials.

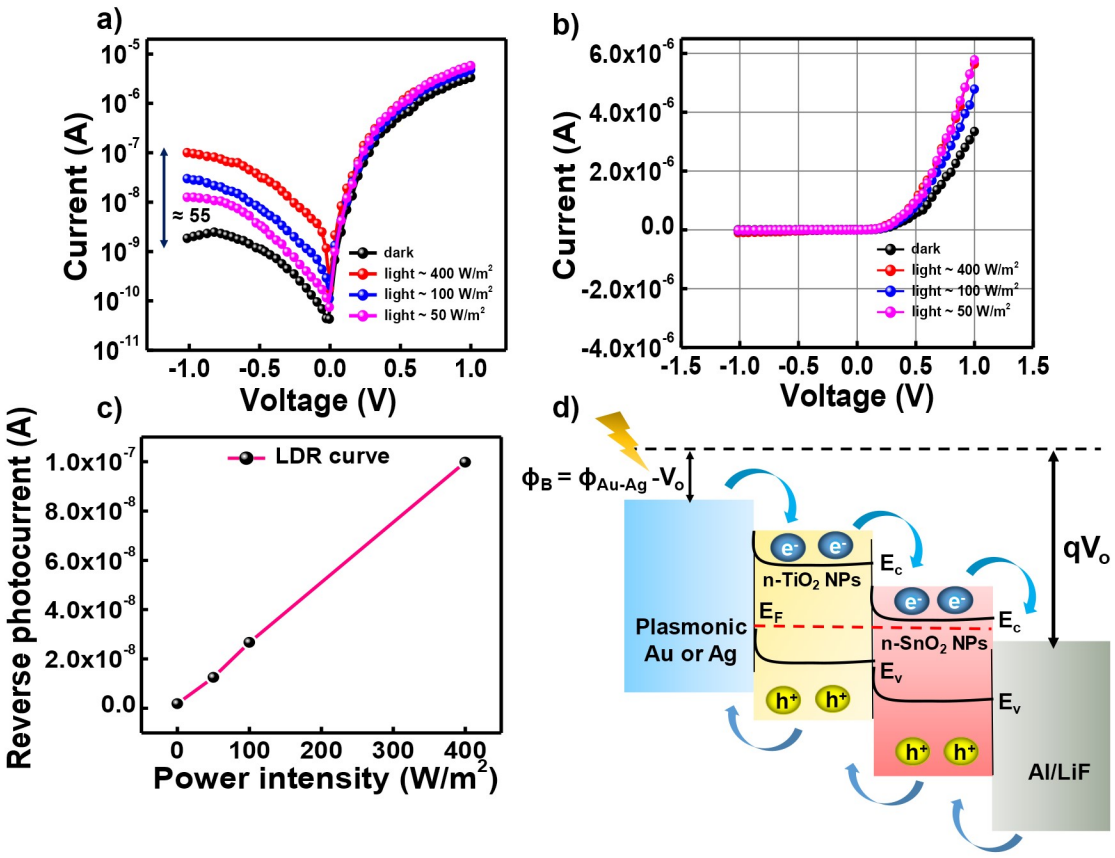

Figure 5.9a) photocurrent generation of plastic compatible Au-Ag transparent plasmonic electrode based photodiode device under dark and light conditions (semi-log plot) **b)** linear I-V plot **c)** reverse photocurrent vs power intensity (LDR curve) **d)** band alignment, band bending and charge separation of this hetero-structure photodiode devices.

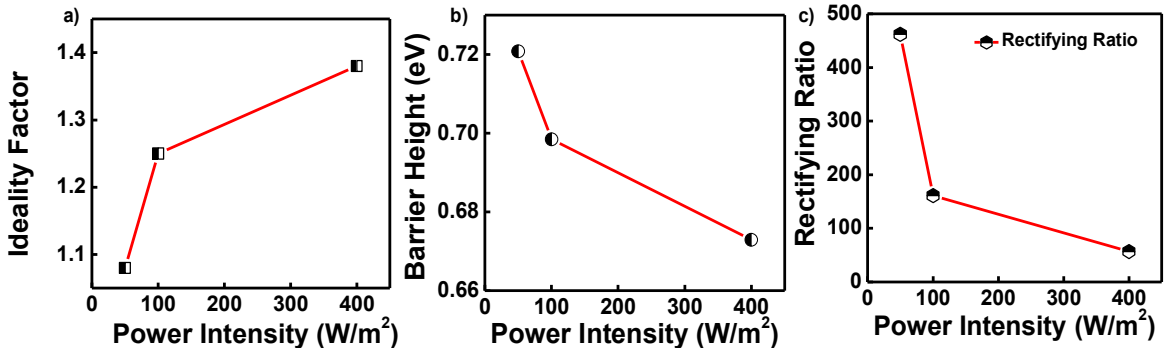

Figure 5.10a) experimental barrier height vs power intensity (Φ_b–P) curve **b)** experimental ideality factor vs power intensity (n-P) curve **c)** experimental rectifying ratio vs power intensity curve of the photodiode

5.3.6 EQE, Responsivity and Detectivity and role of plasmon induced hot electron

The EQE values under different external bias have been measured in the wavelength range of 300 to 1800 nm, as shown in **Figure 5.11a)**. This data implies that EQE value reaches ~ 32.62 % at 750 nm under -2V external bias. Because of the bi-metallic formation of plasmonic Au-Ag NPs, EQE spectra extended upto 1500 nm, which cover entire UV-Vis to NIR spectra region. It can be noted that the EQE spectra of this device is quite similar to the absorption spectra of the 4 nm Au/Ag-TiO_2/SnO_2 NPs film (**Figure 5.3c)**) with exactly same peak position (750 nm) which indicates the photocurrent is mostly generated from the plasmon driven hot electron generation. Responsivity and detectivity of the device is calculated from EQE measurement by using **Equation 1.3** and **1.4** respectively. The variation of photo-responsivity under different external biases is depicted in **Figure 5.11b)**. These results show that a maximum responsivity of 20.23 (A/W) has been achieved at 750 nm with an external bias of -2V. As a plasmonic photodetector, this responsivity data is reasonably higher than earlier reports. Besides, detectivity is another fundamental device parameter that suggests the device sensitivity with respect to the minimum signal that can be detected by the photodetector. The variation of the device's detectivities is shown in **Figure 5.11c)**. The highest detectivity of this heterojunction photodetector that has been calculated is of 1.6×10^{13} Jones at 750 nm under -2 V external bias. As mentioned earlier, there is a

significant amount of photo detection of this plastic based bi-metallic device with a detectivity of 2.33×10^{12} Jones is achievable in the NIR region (wavelength of 1500 nm). It is worth mentioning that the plasmonic absorption peak coincides perfectly with the peak of the detectivity of the device, indicating the hot electron of bimetallic Au-Ag NPs is primarily responsible for this device's photocurrent generation.

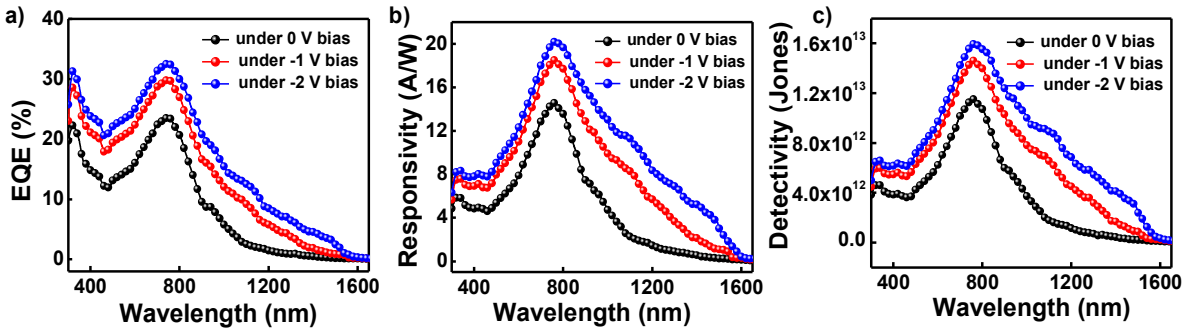

Figure 5.11 device performance of heterostructure photodiode **a)** EQE vs wavelength **b)** extracted R_λ vs wavelength **c)** Extracted D* vs wavelength.

5.3.7 Transient Time Response

Beside device photosensitivity, transient photo response is another key parameter of a photodetector that implies how fast a device can respond and how promptly it can back to its original stage for detecting the next signal. To determine the photo-response of these devices a white light pulse of width and separation of ~ 5 s is illuminated on the device. During this study, the device is subjected to -2V external bias. This transient photocurrent data which is shown in **Figure 5.12a&b)**, reveals that the device's rise and decay time are ~ 16.2 ms and ~ 16.7 ms respectively, indicating the device has fast photo response and recovery time. Furthermore, devices are stored in an ambient atmosphere for a few months, although its photosensitivity and transient time remains almost the same, indicating its very high atmospheric stability.

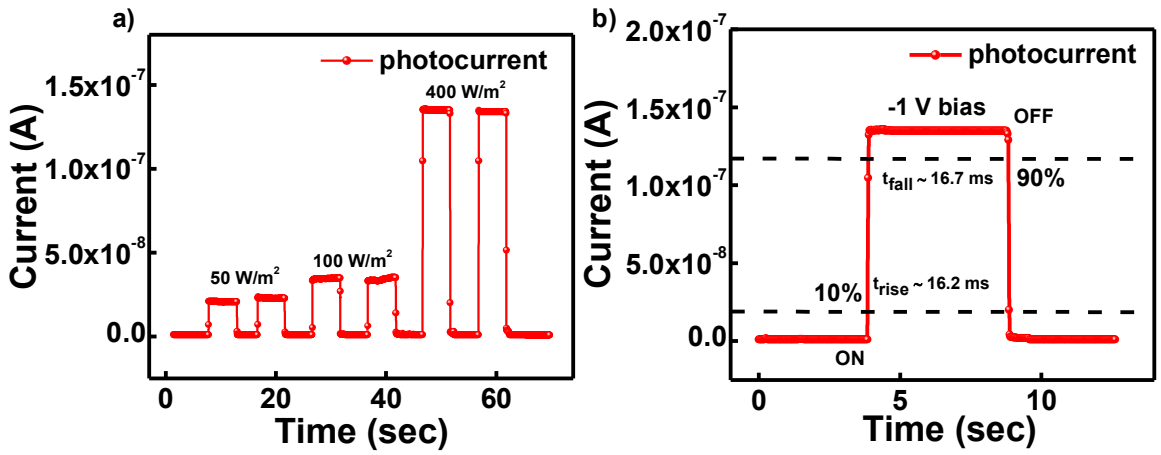

Figure 5.12a) Transient time response of the device **b)** single cycle time response data with rising and decaying times of ~ 16.2 ms and ~ 16.7 ms, respectively.

For a comprehensive assessment of our device's performance, a summary of previously published work on photodetectors based on plasmonic hot electrons is presented in **Table 5.2**. It can be noted that earlier investigations into hot-electron photodetectors have primarily focused on spectral response (R_λ) and the rise-to-fall time ratio (t_{rise}/t_{fall}). Although, important parameters of the hot electron photodetectors are the EQE and D* spectra analysis from where contribution of the hot-electron can be realized, have not been explored in most of the reports. Some earlier works on a hot-electron based photodetector has been listed below. In comparison to other reported hot-electron photodetectors, this flexible plasmonic hot-electron photodetector exhibits a higher responsivity, higher detectivity with fast response speed.

Table 5.2 Comparison of the performance of the current plasmonic hot electrons photodetector with that of other similar devices employing plasmonic hot electrons

Device	λ_{max} (nm)	EQE (%)	R (A/W)	D^* (Jones)	τ_r/τ_f	Ref.
SnO_2 NPs/TiO_2 NPs/(4 nm Au/Ag-TiO_2/SnO_2 NPs)/Plastic	**750**	**32.62**	**20.23**	**1.6×10^{13}**	**16.2/16.7 ms**	**This work**
Porous Ag/TiO_2/Ti	450	–	3.3×10^{-3}	9.8×10^{10}	112/24 μs	[165]
Ag/TiO_2 NTs/FTO	370	–	176.30	–	82/14 s	[172]
Porous Au/Si	–	–	3.5×10^{-3}	–	–	[173]
Au nanorods/Si	–	–	1.0×10^{-5}	–	–	[154]
Au/Pyramid-Si	1200	–	8.2×10^{-3}	1.8×10^{10}	–	[159]

5.4 Conclusions

In conclusion, a cost effective synthesis technique has been developed to fabricate mechanically flexible transparent conductors. For this synthesis, initially a $Li_4Ti_5O_{12}$/SnO_2 NPs heterojunction thin film has been prepared through a solution processed technique with processing temperature of ~100 ºC. Then, the loosely bound Li^+ of $Li_4Ti_5O_{12}$ thin film has been replaced by Ag^+ through an ion-exchange process that forms a Ag-TiO_2 thin film. Thereafter, a thermally evaporated Au of thickness 4 nm is deposited on top of this Ag-TiO_2/SnO_2 NPs thin film, which shows high electrical conductivity (5-10 ohm/□) with ~ 80% average visible transmittance in the range of 500-600 nm wavelength. The electrical conductivity of this film (4 nm Au/Ag-TiO_2/SnO_2 NPs) is significantly higher w.r.t reference

bare plastic substrate Au film (4 nm Au/plastic). Besides, this film also shows a vibrant plasmonic absorption extended up to 1600 nm. By utilizing combined electrical conductivity, optical transparency and plasmonic absorption features of this thin film, a plasmonic photodetector has been fabricated where 4 nm Au/Ag-TiO_2/SnO_2 thin film works as plasmonic electrode as well as photocurrent harvesting materials and LiF/Al substrate as counter electrode. Device shows a very high photosensitivity to the visible light. Besides, it has been observed that the EQE spectra of this device has a great similarity with the absorption spectra of 4 nm Au/Ag-TiO_2/SnO_2 thin film with same absorption and EQE peak position (750 nm) that reveal the contribution of plasmonic hot electron in the photocurrent generation of the device. Device shows EQE, photo responsiveness, and detectivity of values 32.62%, 20.23 A/W, and 1.6×10^{13} Jones, respectively at (750 nm). Moreover, these devices show fast photo response with a rise and decay times of 16.2 ms and 16.7 ms respectively. Overall performance of this plasmonic photodetector is significantly higher than the previous report that gives a visible way to fabricate reliable hot electron based photodetectors.

Chapter 5

Mechanically Flexible Au-Ag bimetallic Plasmonic Transparent Conductor for Boosting Efficiency of Organic Solar Cell

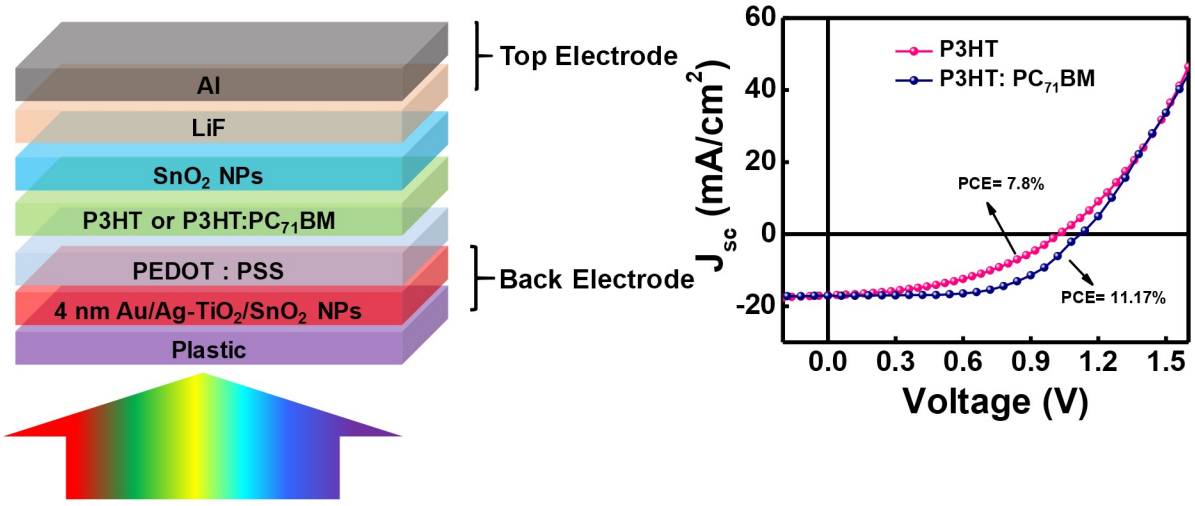

This work is the continuation of previous chapter 5, where bimetallic Au-Ag film is used as a back electrode of plasmonic organic solar cells (POSCs). In recent years, there has been great interest in the utilization of plasmons, or free electron oscillations of MNPs, to increase the efficiency of both organic and inorganic thin film optoelectronic devices. This has been driven by the possibility of employing thin plasmonic MNPs layer in order to increase photo absorption by light trapping in photovoltaic or other opto-electronic devices. In this particular work, I fabricated donor only (P3HT) and donor-acceptor bulk heterojunction (P3HT: PCBM) solar cell using Au-Ag plasmonic thin film as a back electrode. Experimental data indicates a promising enhancement in solar cell performance parameters, including both the open circuit voltage (V_{OC}) and short circuit current density (J_{SC}), has been observed for single layer P3HT and blended P3HT:$PC_{71}BM$ based organic solar cell devices. The observed V_{OC} for donor only and BHJ solar cell reaches to 1.00 and 1.13 V respectively, ensuring tandem cell formation due to the plasmonic Au-Ag film. As a consequence, the PCE values of these two cells reaches to 7.8 % and 11.17% respectively which are record efficiency with these materials combination. These results suggest a unique way to boost PCE of thin film solar cells by utilizing hot carriers of plasmonic Au-Ag thin film that not only works as TC of the device but also increases its V_{OC} by ~ two times.

5.5 Introduction

Transparent conductors (TCs) are in high demand in modern time due to their wide range of applications in electronics, including touch screens, wearable sensors, memory devices, organic light-emitting diodes (OLEDs), solar cells, smart windows etc.[23, 265-269] Traditionally, indium tin oxide (ITO) and fluorine-doped tin oxide (FTO) have dominated the TC market due to their high optical transparency (~ 90%) and low sheet resistance (R_s < 100 Ω/□). However, the scarcity of indium, along other inherent limitations of ITO—such as low mechanical flexibility and complex, costly manufacturing processes has driven the search for alternative TC materials.[116, 117]

To find out the substitute of these metal oxide based TCs, recent studies have focused on next-generation TCs that can provide a balance of transparency, conductivity, mechanical flexibility, and ease of fabrication. Carbon-based materials, including carbon nanotubes and graphene, have garnered attention for their excellent flexibility and optical transparency.[175, 176, 251] However, their electrical conductivity remains lower than that of metals like Ag, Cu, and Au. As a result, metal nanowires and nanoparticle networks have emerged as promising alternatives, particularly for flexible and stretchable electronics, where they offer superior mechanical flexibility, high optical clarity, low sheet resistance, and cost-effective production.[177, 253, 254] Among metals, Ag has emerged as a leading candidate for TCs due to its exceptionally high intrinsic conductivity and low refractive index in the visible spectrum. Ag nanowire networks and oxide/Ag/oxide multilayer films, in particular, have shown significant promise.[181, 255] Copper, though less expensive and conductive, is more chemically reactive, as is Ag, with both materials prone to oxidation.[256, 257] Au, by contrast, offers excellent chemical stability but is limited by lower conductivity and higher cost.[270] To address these stability concerns, researchers have developed core-shell structures that encapsulate metals with chemically inert shells, an approach that enhances the longevity of TCs in a cost-effective manner. Despite advancements, limited studies have explored the use of bimetallic core-shell architectures like Au-Ag, Ag-Cu, and Au-Cu for TC applications, highlighting an area of potential growth.[271, 272]

A critical barrier to achieving high transparency in metal-based TCs is their strong plasmonic absorption, which restricts optical transparency. Nevertheless, plasmonic effects have been harnessed advantageously in solar cells, plasmonic photodetectors, gas sensors, and LEDs.[186, 189] These effects enable hot-electron generation, enhancing photocurrent in devices such as solar cells, photodetectors, and systems for photo-electrochemical hydrogen production.[140, 190] To advance TCs, ongoing research must aim to resolve the balance of optical transparency, electrical conductivity, mechanical durability, and chemical stability. The development of multi-metallic and core-shell nanostructures offers promising pathways to realize high-performance TCs suited to the next generation of flexible and transparent optoelectronic devices.

Plasmonic effects are increasingly explored in solar cell research due to their potential to improve light trapping in organic and inorganic thin-film solar cells, enhancing efficiency.[273-275] The key feature of plasmon resonance is its ability to concentrate conduction electron oscillations within specific spectral ranges. Nevertheless, due to the resonant nature of plasmonic effects, absorption enhancement is limited to specific wavelengths dictated by the NP's size, shape, composition, and local dielectric environment.[76, 276] This enhancement is often offset by parasitic absorption at other wavelengths, reducing efficiency gains. Thus, achieving broadband optical absorption enhancement is essential for advancing plasmonic solar cells beyond the lab.[277, 278] Prior research has focused on theoretical models and experimental setups with random or structured monometallic NPs or gratings requiring precise geometry. While theoretical studies show promising efficiency boosts from metallic NP plasmonic effects, substantial experimental improvements remain elusive, influenced by several factors affecting optical absorption in thin-film solar cells.

Organic photovoltaic devices (OPVs) fabrication is an advancing research field due to their potential as low-cost, lightweight renewable energy sources with promising PCE.[279-281] Since Tang et al.'s 1986 report on the first two-layer OPV[282], significant progress has been made, with continuous improvements in device efficiency through novel materials, device engineering, and architecture. Spin coating is the primary technique for lab-scale OPV fabrication, and state-of-the-art OPVs with donor/acceptor bulk heterojunction (BHJ) or tandem structures now achieve PCEs exceeding 15-20%.[280, 283, 284] The incorporation of plasmonic MNPs has recently been identified as a promising approach to enhance OPV efficiency. This improvement is attributed to increase light trapping and enhanced electrical properties due to the metallic nature of MNPs. Plasmonic NPs can be blended with OPV layers or added as a separate layer, and various synthesis methods, including sol-gel routes and laser nanofabrication, have been explored.[285-288] Numerous studies have examined how factors such as solvent choice, drying rates, annealing, and post-deposition treatments influence layer morphology and PCE. Among these, P3HT:$PC_{71}BM$ BHJs remain prominent in polymer photovoltaic research,[275, 289-291] although new organic polymers are increasingly used to produce efficient BHJs globally.[113, 292] However, literature on achieving high-efficiency P3HT:$PC_{71}BM$ organic solar cells (OSCs) remains limited.

In this section of this chapter, We report the synthesis of Au-Ag bimetallic transparent conducting film on plastic substrate at a low processing temperature (120°C). The as-synthesized Au-Ag bimetallic thin film is highly conductive with sheet resistance as low as 5-6 Ω/□ with more than 80% transparency, which is achieved without any purification steps. Like the earlier section, this Au-Ag film has been developed by depositing 4 nm Au on a pre-deposited Ag-TiO_2/SnO_2 thin film that enables us to achieve a high conducting film with such a low thickness Au deposition. Besides, this transparent-conducting Au-Ag bimetallic film has been used as a back electrode for developing highly efficient organic solar cells. The device has been fabricated on a plastic substrate by using donor only and Donor-acceptor bulk heterojunction geometry. The power conversion efficiency (PCE) of donor only (P3HT) and BHJ (P3HT:PCBM) solar cells are 7.8% and 11.17% respectively, which are record efficiency with this materials combination. These improvements become possible due to enhancement of open circuit voltage by almost double, ensuring a tandem cell formation. Moreover, photocurrent spectra of these devices are broaden from 300 to 1600 nm due to the plasmonic hot carriers of Au-Ag thin film, which is significantly larger w.r.t. it's common photocurrent generation spectral range of 300-700 nm of these organic semiconductor.

5.6 Experimental Section

5.6.1 Preparation of Precursor Solution

The preparation process for ion-conducting dielectric LTO, SnO_2 NPs, PEDOT:PSS, P3HT, and blended P3HT:$PC_{71}BM$ via low cost solution process technique has been explained in **Chapter 2 Section 2.1.1, 2.1.3, 2.1.8, 2.1.9, 2.1.12**.

5.6.2 Fabrication of Au-Ag TC Film and Plasmonic Organic Solar Cells

Bimetallic Au-Ag based TC film has been fabricated on a flexible PET substrate and the fabrication steps has been explained **Chapter 2 Section 2.3.3**, and schematically present in **Figure 2.9**. For fabrication of a photodetector, these optimized mechanically flexible bimetallic Au-Ag TC thin film have been used as transparent bottom electrode to develop NIR active plasmonic photodetector in a photodiode geometry which is schematically present in **Figure 2.11**.

5.7 Results and Discussion

5.7.1 Electrical and Optical Characterization of Flexible Au-Ag Bimetallic Transparent Conductor

Electrical and optical characterization of prepared Au-Ag flexible TC film is discussed earlier in **Chapter 5 Section 5.3.1**.

5.7.2 XRD, Raman, UV-Vis-NIR absorption & PL Spectra

All structural analysis of Au-Ag TC film is discussed in **Chapter 5 Section 5.3.2**.

5.7.3 Surface Morphology (HR-SEM & AFM) & HR-TEM

Surface morphology of prepared film is discussed in details in **Chapter 5 Section 5.3.3.** HR-TEM is done to calculate the particle size of plasmonic NPs and also it tells us about crystal plane of the film which is discussed in **Chapter 5 Section 5.3.4.**

5.7.4 UV-Vis & PL Spectra of P3HT and P3HT: PCBM Film

The UV–Vis absorption spectra of P3HT and blended P3HT:$PC_{71}BM$ are studied in **Figure 5.13a)**. The absorption spectra of P3HT film generally shows a broad absorption in the visible range extended from 450 to 620 nm, while P3HT:$PC_{71}BM$ blend exhibits wider absorption covering from 300 to 620 nm because of $PC_{71}BM$. Interestingly, when these polymers are deposited on top of the prepared TC film (4 nm Au/Ag-TiO_2/SnO_2 NPs), shows a quite broader absorption spectrum, extended up to 1500 nm as shown in **Figure 5.13a).** Here, the LSPR effect of the Au-Ag bimetallic film enhances the light absorption in the stacked film which is realized from the absorption spectra of Au-Ag thin film (Inset of **Figure 5.13a**). The Steady-State Photoluminescence (SSPL) spectra of organic solar cells based on P3HT and blended P3HT: $PC_{71}BM$ provide valuable insights into charge transfer efficiency and quenching mechanism. In pristine P3HT, strong PL is observed in the range of 620–700 nm, corresponding to its excitonic emissions. However, when blended with $PC_{71}BM$, PL is significantly quenched, indicating efficient charge transfer from P3HT (donor) to $PC_{71}BM$ (acceptor), which is essential for effective exciton dissociation. The degree of quenching reflects the efficiency of the heterojunction in facilitating charge

separation. Since $PC_{71}BM$ itself does not exhibit significant PL in the visible range, its presence mainly influences the spectral shape and intensity through its strong electron-accepting properties. Again, as soon organic films are prepared on Au-Ag bimetallic TC film, PL spectrums are blue shifted which is shown in **Figure 5.13b)** as PL peak is observed around 570-590 nm. This observation is mainly due to changes in the local dielectric environment and exciton interactions. The plasmonic effect of the Au-Ag film alters the exciton recombination dynamics, leading to enhanced exciton dissociation and modification of the energy levels.

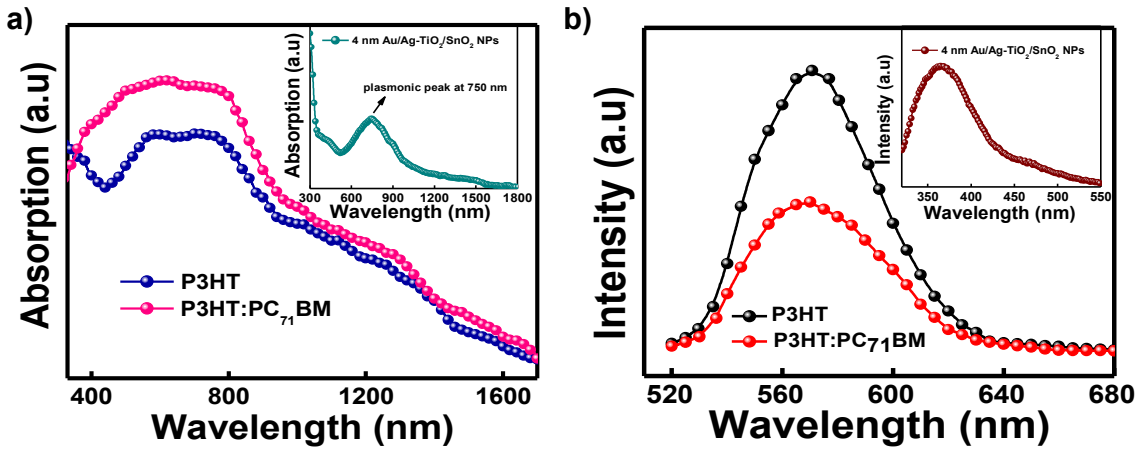

Figure 5.13a) UV-Vis absorption spectra **b)** PL spectra of P3HT and P3HT:PC71BM polymeric film over Au-Ag TC film.

5.7.5 Surface Morphology (HR-SEM & AFM) of P3HT and P3HT: $PC_{71}BM$ Film

Figure 5.14a&b) shows the SEM analysis which reveals significant morphological differences between pure P3HT and P3HT: $PC_{71}BM$ blended films, which directly impacting PCE of solar cells. Pure P3HT films exhibit a smooth morphology with limited charge transport efficiency due to the absence of an acceptor, leading to high recombination losses. Average grain size of P3HT film is around 45-50 nm while in contrast P3HT: $PC_{71}BM$ blends film shows higher average grain size of ~ 50-55 nm, which leads to less grain boundary formation in blended film. Larger grains lead to better polymer crystallinity and improved π-π stacking, which facilitates charge carrier mobility by reducing the trap states. As a result,

it sufficiently reduces recombination losses, result improve J_{sc} and V_{oc} and overall PCE compared to pure P3HT films.

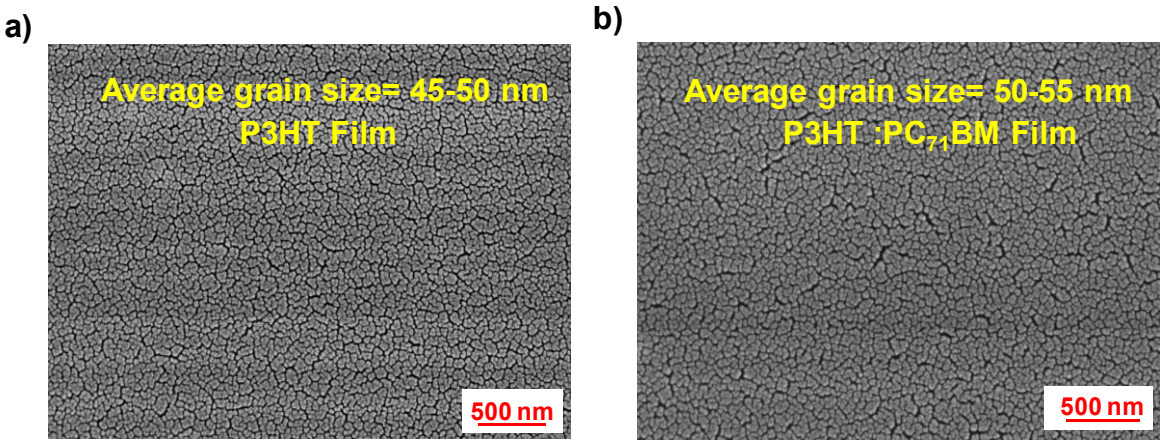

Figure 5.14a&b) HR-SEM image of pure P3HT & blended P3HT: $PC_{71}BM$ polymeric thin film over Au-Ag TC film.

AFM measurement is also performed to investigate the roughness and grown pattern of pure P3HT & blended P3HT: $PC_{71}BM$ polymeric film. The 2D & 3D AFM topographical images of pure P3HT & blended P3HT: $PC_{71}BM$ are shown in **Figure 5.15a,b,c&d**). In pure P3HT films, the AFM image shows a relatively rough surface (r.m.s roughness ~ 3.72 nm) with fine polymer domains, indicating good self-organization but limited charge separation capability. On the other hand, blended P3HT:$PC_{71}BM$ film exhibits distinct nanoscale phase separation, where the surface roughness (r.m.s roughness ~ 3.12 nm) decreases due to the bulk heterojunction formation, leading to a more uniform and compact film morphology. Also, reduced roughness improves the film's contact with the electrode, enhancing charge extraction and reducing interfacial resistance the formation of donor-acceptor domains. Therefore, AFM analysis helps optimize processing conditions to achieve an ideal morphology that enhances charge transport, reduces recombination losses, and improves overall PCE in OPVs.

.

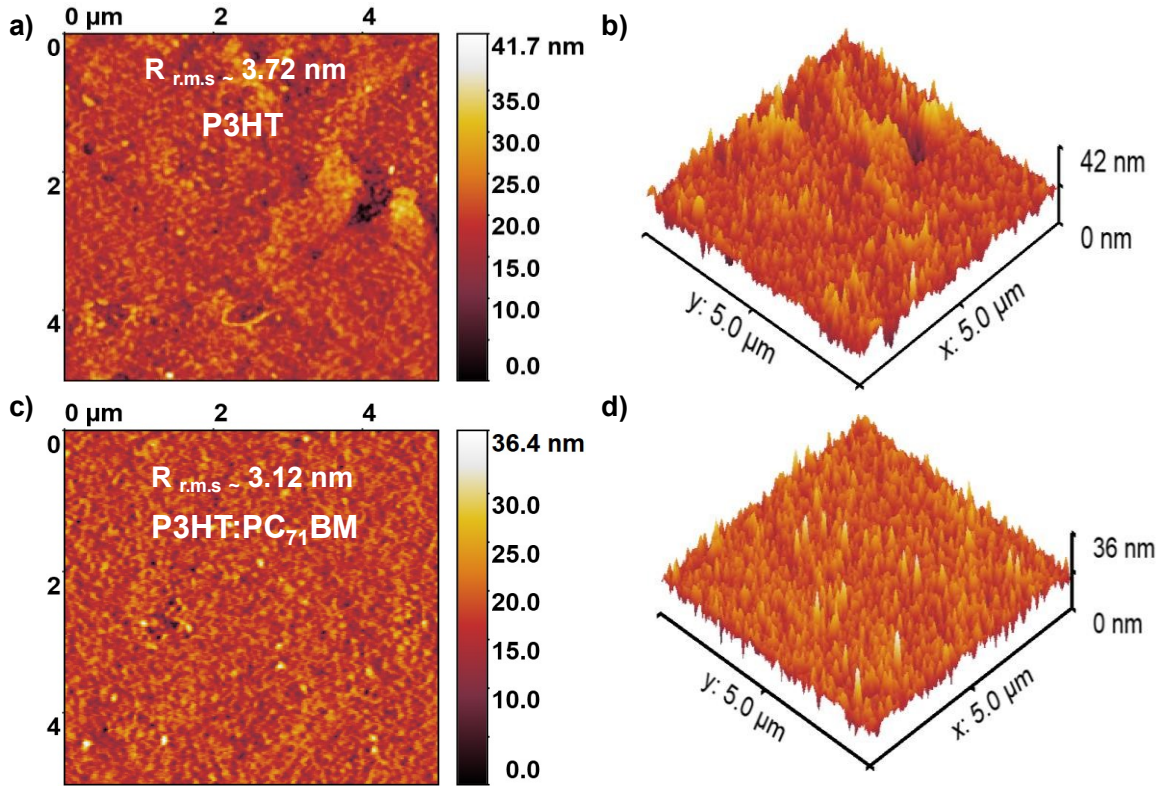

Figure 5.15 Morphological Study by AFM **a)** pure P3HT **b)** blended P3HT:$PC_{71}BM$ film over Au-Ag TC film.

5.7.6 Device Performance of Organic Solar Cells

The photovoltaic properties of pure P3HT and blended P3HT:$PC_{71}BM$ are investigated by fabricating devices with an inverted structure (plastic/SnO_2 NPs/Ag-TiO_2/4 nm Au/PEDOT:PSS/active layer/SnO_2 NPs/LiF/Al) with an active exposure area of 0.09 cm^2. **Figure 5.16a)**, shows a semi-log plot of the dark J–V characteristics for both devices. The ideality factor (η) of the devices are calculated from these plots by using the **Equation 2.8**. As estimated, the η values of are 1.7 and 2.3, for P3HT and P3HT:$PC_{71}BM$ devices, which are moderate to the high bias regions, where space charge limited current (SCLC) is predominant.[79] The photovoltaic performance of these devices are tested under ambient conditions with an illumination 1 sun white light that is shown in **Figure 5.16b).** The details of photovoltaic device parameters for both devices are shown in **Table 5.3,** indicating devices have very similar short circuit current with a density of ~17.5 mA/cm^2 which is reasonably high. Besides, it is very worth to note that the V_{OC} of the P3HT:$PC_{71}BM$ devices

is ~1.13 V which is almost double reported w.r.t the reported works on this class of organic solar cell. Again, V_{OC} of the P3HT is ~1.0 V which is hardly reported in literature. As a consequence, the PCE of P3HT and P3HT: $PC_{71}BM$ devices reaches to ~7.8% and 11.2% respectively which are record efficiency solar cell that are reported with these molecules. We have repeatedly tested the device under identical conditions and consistently observed similar performance, confirming the reliability of the results. The unusually high power conversion efficiency (PCE) primarily originates from the plasmonic bottom electrode. Unlike a conventional transparent or metallic electrode, the plasmonic electrode not only facilitates charge collection but also actively absorbs incident light through LSPR. This plasmonic absorption contributes directly to the photocurrent generation, in addition to the photocurrent produced by the active organic layer (P3HT:$PC_{71}BM$). Because both the plasmonic electrode and the organic layer act as photoactive components, the device essentially behaves like a tandem solar cell without requiring two separate junctions. The plasmonic electrode enhances light–matter interactions and broadens the absorption window, while the organic layer provides the standard excitonic contribution. The combined effect leads to an improvement in both photocurrent and photovoltage. In particular, the open-circuit voltage (Voc) shows a remarkable increase compared to that of a standard P3HT:$PC_{71}BM$ device, highlighting the synergistic role of the plasmonic electrode in boosting overall device efficiency.

In addition to the J−V characteristics, I investigated the EQE spectra of the devices which is shown in **Figure 5.16c).** It also can be noted that spectral range of these devices are extended up to 1500 nm wavelength which is very significantly higher than the reported EQE spectra of the P3HT:$PC_{71}BM$ BHJ devices that commonly exist within the spectral range of 700 nm. This broadening of the EQE spectra originates from the hot carriers of the plasmonic Au-Ag film, present as a back electrode. To validate the NIR sensitivity of the devices, IR light of peak emission spectra of ~ 980 nm is illuminated on both the devices that shows a large variation of photocurrent. The transient photoresponse of the P3HT:$PC_{71}BM$ devices is with a time interval of ~ 5 sec is shown in **Figure 5.16d),** indicating large variation of device current with reasonably fast device response, gave us evidence of generating photocurrent in NIR region.

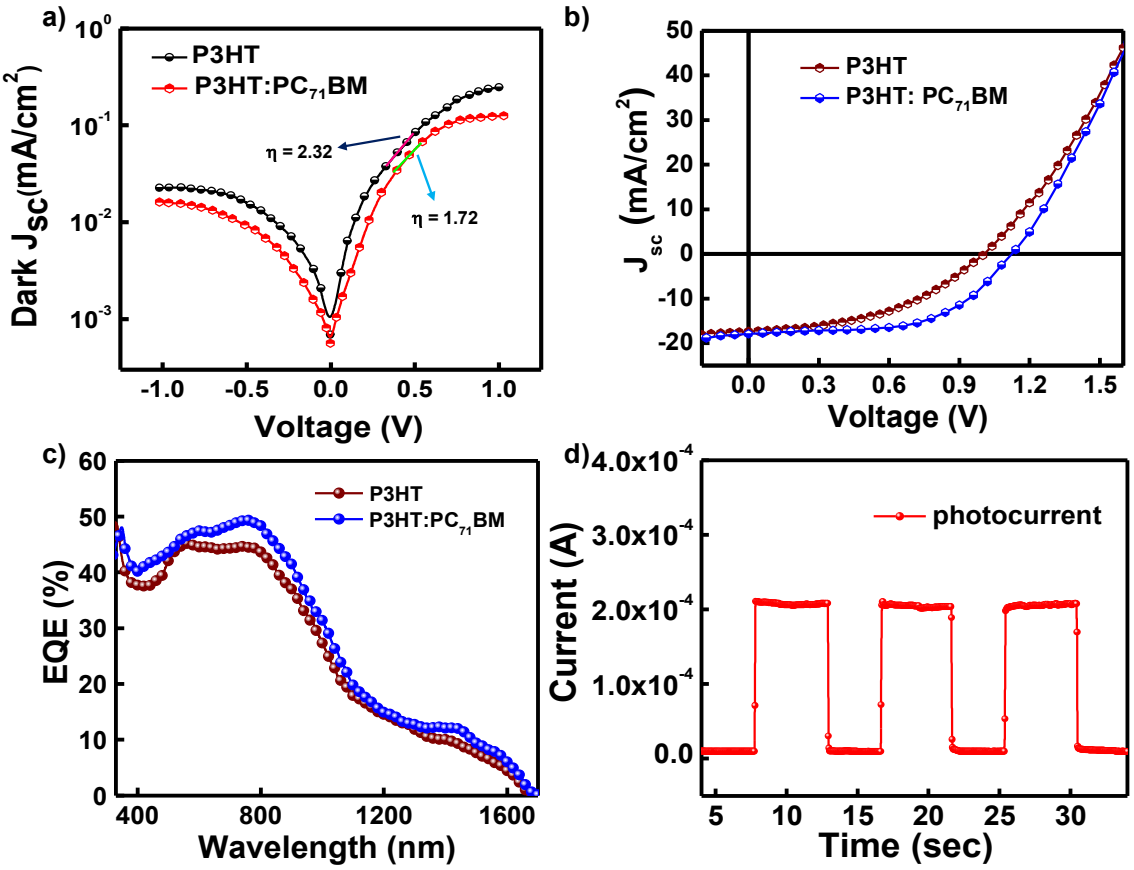

Figure 5.16 device characterization result **a)** dark J-V **b)** J-V under 1 Sun light **c)** EQE vs wavelength **d)** photoresponse with IR light.

Table 5.3 Device Parameter of Calculated Plasmonic Organic Photovoltaics

Active Material	J_{sc} (mA/cm^2)	V_{oc} (V)	FF (%)	PCE (%)
P3HT	17.42	1.01	44.32	7.8
P3HT:PC_{71}BM	17.89	1.13	55.25	11.17

To realize the origin of enhancement of V_{OC} of these devices, I fabricated a reference device without any organic semiconductor, keeping all other components same. The schematic presentation of this reference device is given in the inset of the **Figure 5.17a)**. The J-V

characteristics of this reference device is shown in **Figure 5.17a)**, indicating without any organic semiconductor it can works as a solar cell with a J_{sc} and V_{oc} and PCE of 9.56 ma/cm^2, 0.44 v and 1.36% respectively shown in **Table 5.4**. The EQE spectra of this reference device shows an intense photocurrent generation up to the wavelength of ~1600 nm which is similar to the P3HT and P3HT:$PC_{71}BM$ devices (**Figure 5.17b)**). The J-V characteristics and the EQE spectra of the reference device, clearly implies a tandem cell formation in both the P3HT and P3HT:$PC_{71}BM$ based device where 4 nm Au/Ag-TiO_2/SnO_2 NPs/PEDOT:PSS works as 1st cell which is connected in series with the P3HT:$PC_{71}BM$ (or P3HT)/SnO_2/LiF/Al that works as 2nd cell, resulting an addition of V_{OC} and enhancement photocurrent spectra up to 1600 nm.

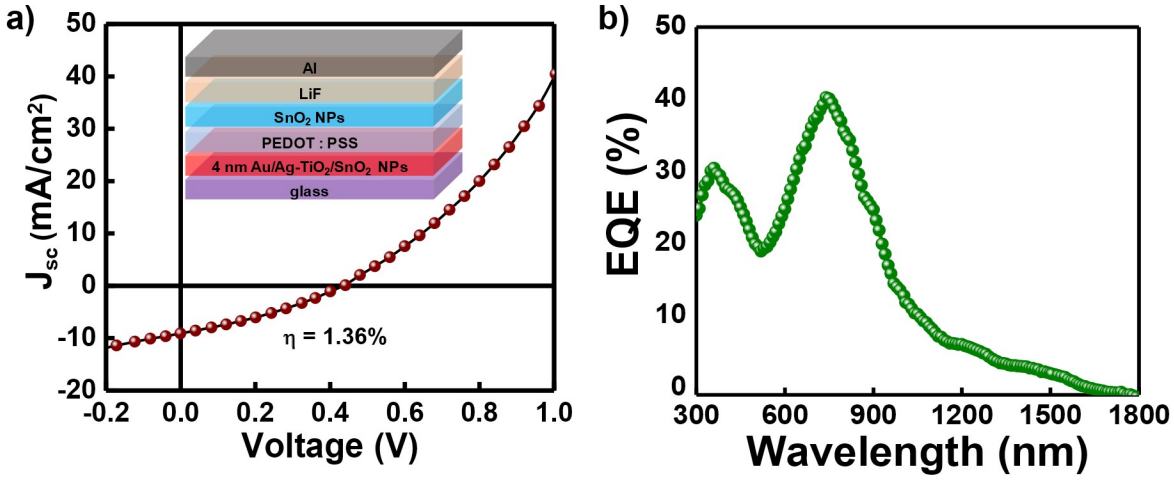

Figure 5.17 device performance of Au-Ag TC film based solar cell without active organic layer **a)** J-V curve under 1 sun light **b)** EQE vs wavelength.

Table 5.4 Device Parameter of Calculated Au-Ag TC Film Based Photovoltaics

J_{sc} (mA/cm^2)	V_{oc} (V)	FF(%)	PCE (%)
9.36	0.44	33.28	1.36

Despite tremendous gains in photovoltaic performance in OSCs, increased stability and repeatability remain a critical concern for practical applications. For that, we checked

reproducibility of the device performance by fabricating atleast 15 small area (0.25 cm^2) P3HT & P3HT:$PC_{71}BM$ based devices. Here, we have shown the histogram plots in **Figure 5.18a)** and the distribution of the data points for champion devices based on P3HT & P3HT:$PC_{71}BM$ active layer. From figure, we found that P3HT based device shows a PCE ranging 7.3 to 8.1%, whereas blended P3HT:$PC_{71}BM$ shows a distribution of PCE ranging from 10.8 to 11.6%. The distribution peak of blended BHJ devices is a little bit higher than that of single organic layer based devices. So, from the overall results, we can conclude that blended BHJ polymeric devices shows better reproducibility and, performance wise, can compete with other air stable organic photovoltaics.

The stability of the fabricated solar cells is an important topic to consider. We analyzed the self-life-testing experiment, which demonstrated the long-term stability of the fabricated cells. The self-life of the produced cells is determined by evaluating and recording the PCE of devices after exposing them to ambient air and room temperature. All the devices are stored in an ambient desiccator (humidity <40% and room temperature 25°C). The J−V measurement is carried out over 720 hours until the produced cell revealed a PCE drop of more than 20% from the initial value. All measurements are typically taken every five days, with the cells exposed to the solar simulator's light for less than one minute to avoid the degrading effect of POSCs. **Figure 5.18b)** shows the change in PCE of the devices with time (t) in ambient circumstances. Blended film shows a better stability where it maintains PCE of 80% up to 600 h.

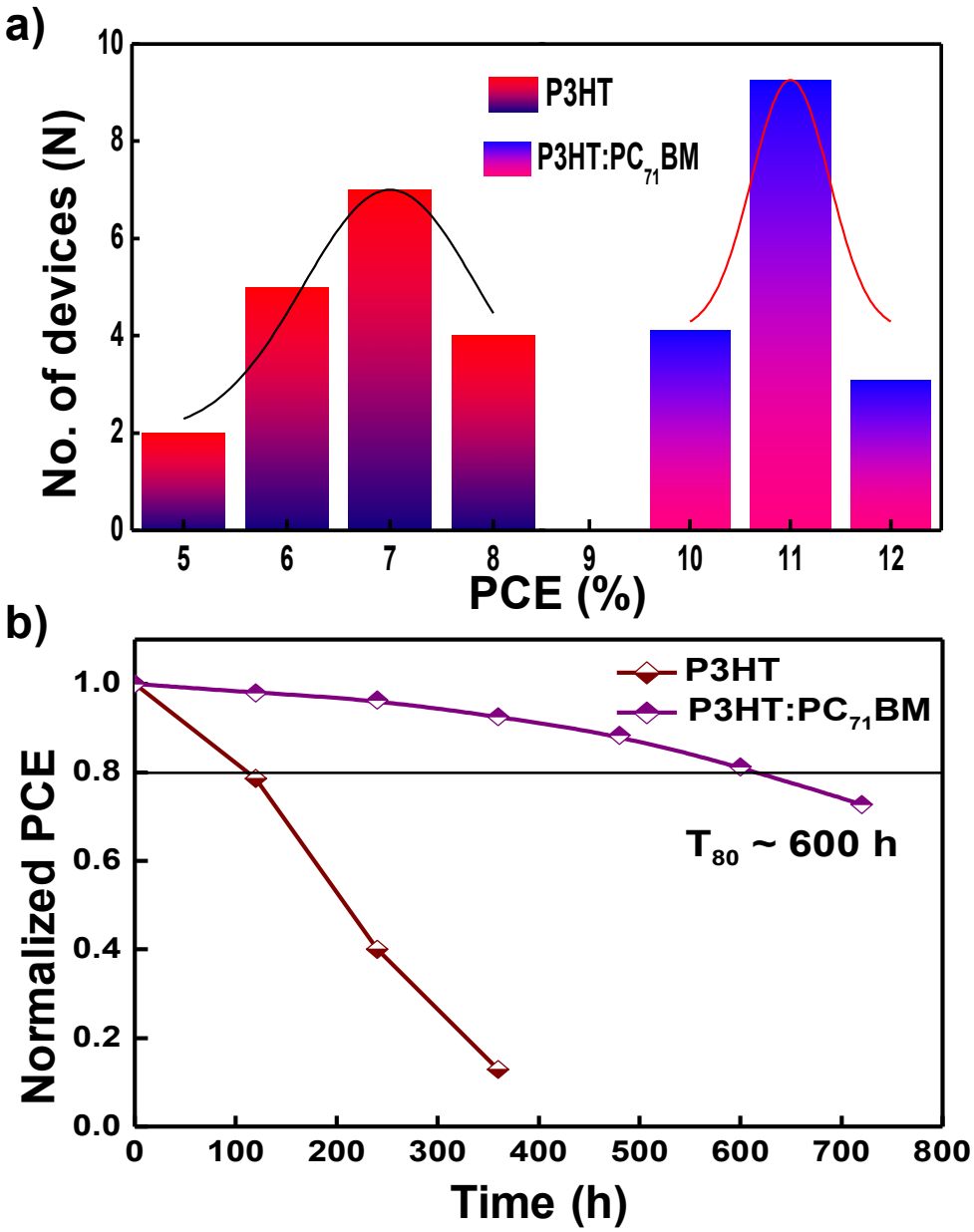

Figure 5.18a) reproducibility and **b)** air stability data of prepared plasmonic organic solar cell devices

5.8 Conclusion

We have successfully developed a solution process low-cost synthesis technique by depositing LTO/SnO_2 NPs based thin film on mechanically flexible plastic substrate at low

temperature by combined heating (at 100 ^{o}C) and UV illumination. Then, the loosely bound Li^{+} of this thin film has been replaced by Ag^{+} through an ion-exchange process that forms a Ag-TiO_2 thin film. A thermally evaporated 4 nm Au is deposited on top of this Ag-TiO_2/SnO_2 NPs thin film, which shows high electrical conductivity (5-10 ohm/□) and over 80% average visible transmittance in the range of 500-600 nm wavelength. This high electrical conductivity of the film appears due to the percolated growth of nanostructure Au-Ag NPs film during thermal evaporation. This film also shows a vibrant plasmonic absorption in the UV-Vis-NIR region. By utilizing combined optical transparency and plasmonic absorption features of this thin film, a plasmonic organic solar cell has been fabricated using this transparent electrode as a bottom electrode, where 4 nm Au/Ag-TiO_2/SnO_2 thin film works as plasmonic electrode and LiF/Al substrate as top electrode. Device shows a record PCE of 7.8% with pure P3HT and 11.17% with blended P3HT:PC_{71}BM based film, which is unusually high w.r.t the ITO coated device. A reference device without the organic semiconducting layer shows a solar cell behavior with a PCE of 1.36% to ensure a separate cell formation by the plasmonic Au-Ag based TC which is connected in series with the fabricated organic solar cell. As a result, V_{oc} improved by 1.5 times which ensures tandem cell formation in presence of an organic active layer. This P3HT: PCBM BHJ organic layer shows an excellent ambient (25 °C, 40–60% RH) stability (retained 80% of the initial PCE) up to 600 h of storage without encapsulation.